Ellipsoidal shape fluctuations of the compound nucleus

R. J. Charity
Department of Chemistry, Washington University, St. Louis, Missouri 63130
(Received 24 July 2001; published 20 November 2001)

Hot rotating compound nuclei are modeled as ellipsoidally shaped liquid drops. A formalism for the determination of their equilibrium shape distribution is presented. Commonly used metrics associated with the volume element in deformation space are derived with a discussion of their underlying assumptions. Example calculations of shape distributions are presented. These distributions are not characterized by any one type of shape in particular; the full range of deformations from oblate to prolate are populated including spherical and triaxial deformations. However the tail of the distributions extending towards highly deformed prolate configurations is more pronounced especially at the higher angular momenta. The shape of the Coulomb-barrier distributions for the evaporation of charged particles from the nuclear surface, averaged over the equilibrium distribution of shapes, is calculated and its relevance for the understanding of the yield of low-energy α particles observed in evaporation spectra is discussed.

DOI: 10.1103/PhysRevC.64.064610 PACS number(s): 25.70.Gh, 24.60.Dr

I. INTRODUCTION

Thermal fluctuations in the shape of a compound nucleus are an important ingredient in understanding the energy spectra of both charged particles and gamma rays emitted as the nucleus cools. The role of such fluctuations in determining the shape of the gamma-ray spectrum in the region of the giant dipole resonance has been addressed in Refs. [1–4]. Recently, statistical-model calculations incorporating only spheroidal-shape fluctuations reproduced experimental α-particle kinetic-energy spectra measured for a number of compound systems with $A>150$ and excitation energies of $\lesssim 100$ MeV [5]. These calculations were found to account for the experimental yield of low-energy α particles which are not predicted in standard statistical-model calculations for evaporation from spherical systems. In these calculations, low-energy particles are evaporated predominately from the population of highly deformed prolate systems, for which the Coulomb-barrier distribution extends down low in energy for emission from the system's tips. At higher excitation energies these calculations with spheroidal fluctuations were unable to account for the low-energy α-particle yield measured in Ni+Mo reactions [5]. However, real compound nuclei are not constrained to spheroidal shapes. The consideration of other important shape degrees of freedom, when determining the thermal shape distributions at high excitation energies, may increase the probability for the larger deformations, which will have important consequences for the Coulomb-barrier distributions.

As part of an eventual aim of incorporating ellipsoidal-shape fluctuations into evaporation calculations, this work focuses on the formalism for determining the equilibrium shape distributions for hot rotating ellipsoidally shaped systems where shell and pairing effects are washed out and quantum shape fluctuations are small and can be neglected. Other treatments of ellipsoidal-shape distributions [1–4,6–9] make use of two forms for the metric associated with the differential volume element in deformation shape. In Sec. II, the development of a formalism for shape distributions is presented with attention given to the assumptions necessary for the derivation of these metrics. Calculated distributions for a number of example systems are presented in Sec. III along with a comparison of the Coulomb-barrier distributions associated with α-particle emission from equilibrium distributions of spheroidally and ellipsoidally shaped systems. Finally the conclusions of this work are presented in Sec. IV.

II. STATISTICAL THEORY OF SHAPE FLUCTUATIONS

For a system constrained to have an ellipsoidal shape, the radii at the principal axes can be defined by Bohr's β-γ parametrization [10,11] as

$$R_x = R_0(\beta,\gamma)\left[1+\sqrt{\frac{5}{4\pi}}\beta\cos\left(\gamma-\frac{2\pi}{3}\right)\right], \quad (1)$$

$$R_y = R_0(\beta,\gamma)\left[1+\sqrt{\frac{5}{4\pi}}\beta\cos\left(\gamma+\frac{2\pi}{3}\right)\right], \quad (2)$$

$$R_z = R_0(\beta,\gamma)\left[1+\sqrt{\frac{5}{4\pi}}\beta\cos\gamma\right]. \quad (3)$$

The term $R_0(\beta,\gamma)$ was introduced by Kaniowska *et al.* [12] to conserve volume for large deformations,

$$R_0(\beta,\gamma) = \frac{R_{00}}{\left[1-\frac{15}{16\pi}\beta^2+\frac{1}{4}\left(\frac{5}{4\pi}\right)^{3/2}\beta^3\cos(3\gamma)\right]^{1/3}}, \quad (4)$$

where R_{00} is the radius for a spherical shape.

The shape of an ellipsoid can be uniquely defined by a point in the pie sector where β is the radius parameter and γ is the angular coordinate [11]. This pie sector is bounded by the angles $\gamma=0$ and $\gamma=\pi/3$ which correspond to prolate and oblate spheroids, respectively. All other intermediate values of γ correspond to deformations which are not axially symmetric.

The state of an ellipsoid can be specified by the shape coordinates β,γ and the three Euler angles ϕ, θ, and ψ giving the orientation of the ellipsoid's principal axes relative to an external reference frame. At each β,γ point, the differential phase space available to an ellipsoid with total collective energy E can be expressed in terms of these coordinates and their corresponding canonical momenta P_β, P_γ, P_ϕ, P_θ, and P_θ from the microcanonical partition function as

$$W(E,\beta,\gamma)d\beta\,d\gamma = \int dP_\beta \int dP_\gamma \int d\phi \int dP_\phi \int d\theta \int dP_\theta \times \int d\varphi \int dP_\varphi \delta(E-E_{\rm coll})d\beta\,d\gamma. \quad (5)$$

The integrations are over all possible values of the coordinates and momenta. The total collective energy

$$E_{\rm coll}=V(\beta,\gamma)+E_{\rm rot}(\beta,\gamma,P_\phi,P_\theta,P_\varphi)+E_k(\beta,\gamma,P_\beta,P_\gamma) \quad (6)$$

can be subdivided into the contributions from the potential energy for the deformation V, the rotational kinetic energy $E_{\rm rot}$, and the kinetic energy associated with changes in deformation E_k. The five coordinates for the ellipsoid represent a small fraction of the large number of collective and intrinsic degrees of freedom available to the nucleus. Let the level density associated with the remaining degrees of freedom be represented by ρ.

The distribution of compound nuclear shapes will be defined in terms of a probability p per unit area in the pie sector. This probability can be obtained from convoluting the phase space associated with the ellipsoid in Eq. (5) with the level density ρ. The probability associated with the differential area element $\beta\,d\beta\,d\gamma$ in the pie sector is thus defined to be

$$p(E^*,\beta,\gamma)\beta\,d\beta\,d\gamma=\int_0^{E^*} dE\,\rho(E^*-E)W(E,\beta,\gamma)d\beta\,d\gamma \quad (7)$$

$$=K\int dP_\beta \int dP_\gamma \int d\phi \int dP_\phi \int d\theta \times \int dP_\theta \int d\varphi \int dP_\varphi\,\rho(U)d\beta\,d\gamma, \quad (8)$$

where K is a normalization constant and $U=E^*-E_{\rm coll}$. It is useful in evaluating this expression to transform from the momenta P_ϕ, P_θ, P_φ to the more familiar angular-momentum projections J_x, J_y, and J_z along the principal axes using the Jacobian $\sin\theta$. The integration over the Euler angles can then be performed giving a constant term that can be incorporated into K, i.e.,

$$p(E^*,\beta,\gamma)\beta\,d\beta\,d\gamma = K\int dP_\beta \int dP_\gamma \int dJ_x \int dJ_y \int dJ_z\,\rho(U)d\beta\,d\gamma. \quad (9)$$

At high excitation energies, the level density can be expanded as

$$\rho(E^*-V-E_{\rm rot}-E_k)\approx\rho(E^*)\exp\left(-\frac{V+E_{\rm rot}+E_k}{T}\right), \quad (10)$$

where the nuclear temperature is

$$\frac{1}{T}=\frac{d\ln\rho}{dU}. \quad (11)$$

For a Fermi-gas level density, the temperature can be expressed in terms of the level-density parameter a as

$$T\approx\sqrt{\frac{E^*}{a}}. \quad (12)$$

This expansion gives us the canonical distribution function

$$p_c(T,\beta,\gamma)\beta\,d\beta\,d\gamma = K\int dP_\beta \int dP_\gamma \int dJ_x \int dJ_y \int dJ_z \times\exp\left(-\frac{V+E_{\rm rot}+E_k}{T}\right)d\beta\,d\gamma, \quad (13)$$

where the term $\rho(E^*)$ has again been incorporated into the normalization constant K.

Following Bohr [10,11], the kinetic energy E_k can be expressed in terms of three inertia parameters, i.e.,

$$E_k=\frac{1}{2}D_{\beta\beta}\dot\beta^2+D_{\beta\gamma}\dot\beta\dot\gamma+\frac{1}{2}D_{\gamma\gamma}\dot\gamma^2 =\frac{1}{D^2}\left(\frac{1}{2}D_{\gamma\gamma}P_\beta^2-D_{\beta\gamma}P_\beta P_\gamma+\frac{1}{2}D_{\beta\beta}P_\gamma^2\right), \quad (14)$$

where

$$D^2=D_{\beta\beta}D_{\gamma\gamma}-D_{\beta\gamma}^2. \quad (15)$$

The rotational energy can be expressed in terms of the moments of inertia $\mathcal{I}_x$, $\mathcal{I}_y$, $\mathcal{I}_z$ about the three principal axes as

$$E_{\rm rot}=\frac{J_x^2}{2\mathcal{I}_x(\beta,\gamma)}+\frac{J_y^2}{2\mathcal{I}_y(\beta,\gamma)}+\frac{J_z^2}{2\mathcal{I}_z(\beta,\gamma)}. \quad (16)$$

The integrations over the momentum variables are easily performed for this canonical distribution giving

$$p_c(T,\beta,\gamma)\beta\,d\beta\,d\gamma = K\exp\left[-\frac{V(\beta,\gamma)}{T}\right] \times D(\beta,\gamma)\sqrt{\mathcal{I}_x(\beta,\gamma)\mathcal{I}_y(\beta,\gamma)\mathcal{I}_z(\beta,\gamma)}\,d\beta\,d\gamma, \quad (17)$$

where yet again constant terms have been absorbed in K. The term $D\sqrt{\mathcal{I}_x\mathcal{I}_y\mathcal{I}_z}d\beta\,d\gamma = d\tau$ is the metric for this problem, and although it has been derived from the classical partition function, is has a more general application. For example, it was also derived by Kumar and Baranger [13] in their solution to the wave functions for the ellipsoid's motion. It is important to note that the value of the metric depends on the deformation dependence of the inertias.

For inertias $D_{\beta\beta}$, $D_{\gamma\gamma}$, and $D_{\beta\gamma}$, which are associated with changes in shape, the expression obtained by Kaniowska *et al.* [12] for irrotational flow are deemed appropriate at high excitation energies. For the rotational motion, we will consider both rigid-body values

$$\mathcal{I}_x^{RB} = \frac{(R_y^2+R_z^2)}{2R_{00}^2}\mathcal{I}_0, \quad \mathcal{I}_y^{RB} = \frac{(R_x^2+R_z^2)}{2R_{00}^2}\mathcal{I}_0,$$

$$\mathcal{I}_z^{RB} = \frac{(R_x^2+R_y^2)}{2R_{00}^2}\mathcal{I}_0, \quad (18)$$

and values associated with irrotational flow [11],

$$\mathcal{I}_x^{IR} = \left(\frac{R_y^2-R_z^2}{R_y^2+R_z^2}\right)^2\mathcal{I}_x^{RB},$$

$$\mathcal{I}_y^{IR} = \left(\frac{R_x^2-R_z^2}{R_x^2+R_z^2}\right)^2\mathcal{I}_y^{RB}, \quad \mathcal{I}_z^{IR} = \left(\frac{R_x^2-R_y^2}{R_x^2+R_y^2}\right)^2\mathcal{I}_z^{RB}, \quad (19)$$

where $\mathcal{I}_0$ is the spherical rigid-body value. The rigid-body values are expected to be more appropriate at high excitation energies, but the irrotational values will also be considered as they allow comparison with other studies. For small deformations, one can expand the expressions for the inertias about $\beta=0$ and obtain

$$d\tau^{RB} \propto \left(1+\frac{95}{32\pi}\beta^2 - \frac{295}{384}\sqrt{\frac{5}{\pi^3}}\cos 3\gamma\,\beta^3\right)\beta\,d\beta\,d\gamma \quad (20)$$

for rigid-body rotation and

$$d\tau^{IR} \propto \beta^4|\sin 3\gamma|\,d\beta\,d\gamma \quad (21)$$

for inertias associated with irrational flow. To lowest order, these metrics are $\beta\,d\beta\,d\gamma$ and $\beta^4|\sin 3\gamma|\,d\beta\,d\gamma$. These two forms are commonly used in other treatments of ellipsoidal-shape distributions [1–4,6–9]. The difference between these metrics is entirely due to the assumed values for the moments of inertia. Both metrics include the angular-momentum orientation degree of freedoms as in both cases the integration over all values of J_x, J_y, and J_z has been performed. In fact, both metrics include contributions from all absolute values of angular momenta and neither is valid for large deformations. Use of either form must be consistent with these assumptions.

The distribution function just presented may not be particularly useful as most applications of shape fluctuations require that the angular momentum or its distribution be specified. If all three components of the angular momentum J_x, J_y, J_z are constrained, then after removing the integrations over these variables, the metric is simply $d\tau \propto D\,d\beta\,d\gamma$, which, for small β, approaches

$$d\tau \propto \left(1+\frac{25}{16\pi}\beta^2 - \frac{5}{12}\sqrt{\frac{5}{\pi^3}}\cos 3\gamma\,\beta^3\right)\beta\,d\beta\,d\gamma. \quad (22)$$

If the absolute value of the angular momentum is constrained, the canonical distribution function becomes

$$p_c(T,J,\beta,\gamma)\beta\,d\beta\,d\gamma = K\int dP_\beta\int dP_\gamma\int dJ_x\int dJ_y\int dJ_z \times\exp\left(-\frac{V+E_{\rm rot}+E_k}{T}\right)\delta[J^2-(J_x^2+J_y^2+J_z^2)]d\beta\,d\gamma. \quad (23)$$

All the integrations can be performed analytically, except one, giving

$$d\tau \propto D\exp\left(\frac{-E_{\rm rot}^1}{T}\right)d\beta\,d\gamma\int_0^1 dx \times\exp\left[-\frac{E_{\rm rot}^3+E_{\rm rot}^2-2E_{\rm rot}^1}{2T}(1-x^2)\right] \times \mathrm{I}_0\left[\frac{E_{\rm rot}^3-E_{\rm rot}^2}{2T}(1-x^2)\right], \quad (24)$$

where I_0 is the modified Bessel function of the first kind and $E_{\rm rot}^i = J^2/2\mathcal{I}_i$ is the energy for rotation about the ith principal axis which are ordered such that $E_{\rm rot}^1 \leqslant E_{\rm rot}^2 \leqslant E_{\rm rot}^3$. The minimum rotational energy for rigid-body rotation is $E_{\rm rot}^1 = E_{\rm rot}^y$ while for irrotational flow $E_{\rm rot}^1 = E_{\rm rot}^x$. For small deformations, the metrics approach

$$d\tau_J^{RB} \propto \left\{1+\frac{\left[25+2\left(\frac{E_{\rm rot}^0}{T}\right)^2+10\frac{E_{\rm rot}^0}{T}\right]}{16\pi}\beta^2 - \frac{\left[-280-4\left(\frac{E_{\rm rot}^0}{T}\right)^3+63\left(\frac{E_{\rm rot}^0}{T}\right)^2-280\frac{E_{\rm rot}^0}{T}\right]}{672}\sqrt{\frac{5}{\pi^3}}\cos 3\gamma\,\beta^3\right\}\beta\,d\beta\,d\gamma \quad (25)$$

or

$$d\tau_J^{IR} \propto \frac{\exp\left(\dfrac{-4\pi E^0_{\rm rot}}{15\beta^2 \sin^2(\gamma - 2\pi/3)T}\right)}{\sqrt{[csc^2(\gamma+2\pi/3)-csc^2(\gamma-2\pi/3)][csc^2(\gamma)-csc^2(\gamma-2\pi/3)]}}\beta^3 d\beta\, d\gamma, \tag{26}$$

where $E^0_{\rm rot}=J^2/(2\mathcal{I}_0)$ is the rotational energy of the rigid spherical system. Note that for rigid-body rotation, the metric, to lowest order, is $\beta\, d\beta\, d\gamma$ independent of whether or not the angular momentum is constrained.

The deformation potential energy in the liquid-drop model can be expressed in the following form [14]:

$$V(\beta,\gamma)=[B_s(\beta,\gamma)-1]E^0_s+[B_c(\beta,\gamma)-1]E^0_c, \tag{27}$$

where E^0_s and E^0_c are the surface and Coulomb energies for a spherical nucleus and B_s and B_c express the surface and Coulomb energies of a deformed nucleus in units of the respective spherical quantity. The quantities B_s and B_c were derived for ellipsoidal shapes in terms of the incomplete elliptic integrals in Refs. [15,16]. For small values of β,

$$B_s=1+\frac{\beta^2}{2\pi}, \quad B_c=1-\frac{\beta^2}{4\pi} \tag{28}$$

and the canonical distribution function for rigid-body rotation reduces to

$$p_c(T,J,\beta,\gamma)\propto 1+\frac{\beta^2}{16\pi}\left[25+2\left(\frac{E^0_{\rm rot}}{T}\right)^2 + 10\frac{E^0_{\rm rot}}{T}-8\frac{E^0_s}{T}+4\frac{E^0_c}{T}\right]. \tag{29}$$

The distribution function has a maximum at $\beta=0$ so long as

$$E^0_{\rm rot} < \sqrt{(4E^0_s-2E^0_c)T-(5T/2)^2}-5T/2. \tag{30}$$

These expansions cannot be used to describe the full equilibrium shape distribution as large deformations are important. In this case, rather than use the full canonical distribution [Eq. (24)] which was obtained by expanding the level density about E^* in Eq. (10), a better approximation can be obtained by performing the expansion about $E^*-V(\beta,\gamma)-E^1_{\rm rot}(\beta,\gamma)$ for each value of β,γ. The resulting distribution function is

$$p(E^*,J,\beta,\gamma)\propto \rho(U)T\frac{D}{\beta}\int_0^1 dx \times\exp\left[-\frac{E^3_{\rm rot}+E^2_{\rm rot}-2E^1_{\rm rot}}{2T}(1-x^2)\right] \times {\rm I}_0\left[\frac{E^3_{\rm rot}-E^2_{\rm rot}}{2T}(1-x^2)\right], \tag{31}$$

where

$$U=E^*-V(\beta,\gamma)-E^1_{\rm rot}(\beta,\gamma), \quad T=\sqrt{U/a}. \tag{32}$$

In Ref. [5], the distribution of spheroidal shapes was obtained from a summation over the quantum-mechanical rotational levels associated with a rigid spheroid. An equivalent formulation for an ellipsoid is

$$\rho^*(E^*,J,\beta,\gamma)\propto\frac{D}{\beta}\sum_\kappa \rho[E^*-V(\beta,\gamma)-E^{J,\kappa}_{\rm rot}(\beta,\gamma)]T, \tag{33}$$

where now $T=\sqrt{(E^*-V-E^{J,\kappa}_{\rm rot})/a}$ and $E^{J,\kappa}_{\rm rot}$ are the $(2J+1)$ rotational levels of a rigid asymmetric rotor [17] with total angular momentum $J\hbar$. There is no analytical expression for $E^{J,\kappa}_{\rm rot}$ except in the oblate and prolate limits and so the computer code of Jain and Thompson [18] was used. Neither this expression nor the purely classical version, Eq. (31), include the quantum corrections for fluctuations in the shape degrees of freedom and it was found that they both give almost identical results for excitation energies where these corrections are expected to be small.

III. CALCULATIONS

In this section, calculations of equilibrium shape distributions from Eq. (31) will be presented. Following the rotating liquid-drop model (RLDM) [19], the surface and Coulomb energies for spherical systems are taken as [20,21]

$$E^0_s=17.9439\left[1-1.7826\left(\frac{N-Z}{A}\right)^2\right]A^{2/3}\ {\rm MeV}, \tag{34}$$

$$E^0_c=0.7053\frac{Z^2}{A^{1/3}}\ {\rm MeV} \tag{35}$$

and using $r_0=1.2249$ fm, the spherical rigid-body moment of inertia is defined by

$$\frac{\hbar^2}{2\mathcal{I}_0}=\frac{34.540}{A^{5/3}}\ {\rm MeV}. \tag{36}$$

Full calculations, rather than expansions, for D, B_s, B_c, and all moments of inertia are performed. Unless otherwise stated, rigid-body moments of inertia are assumed.

Consider first the example system ^{158}Er. The variation of the inertia parameter D/β and the deformation energy $V(\beta,\gamma)$ are shown in Fig. 1. To gauge the magnitude of the

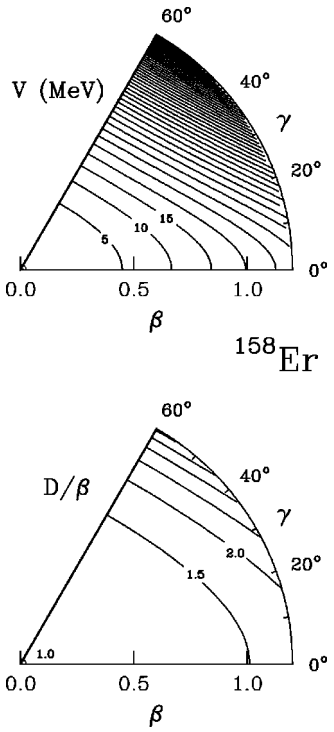

FIG. 1. Contours showing the dependence of the potential energy V and the inertia parameter D/β on the deformation coordinates β and γ for the ^{158}Er system. Contours for D/β are labeled in units of the value for sphericity ($\beta=0$).

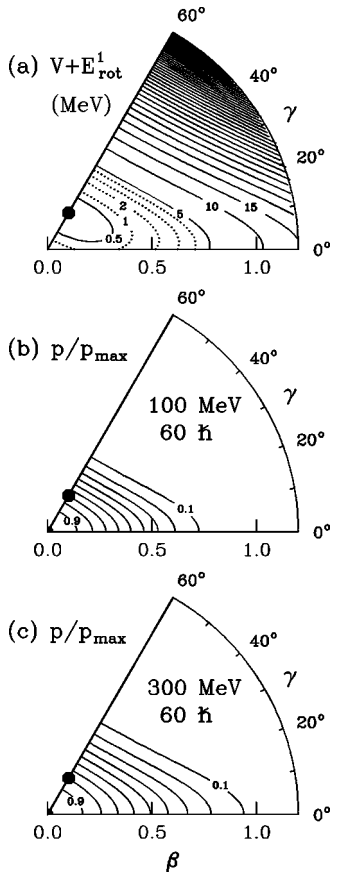

FIG. 2. (a) Contours showing the β,γ dependence of the deformation plus minimum rotational energy $V+E^1_{\rm rot}$ for the ^{158}Er system with $J=60\ \hbar$. The filled point indicates the configuration with the minimum value of $V+E^1_{\rm rot}$ which is 25.2 MeV. The contours are labeled by the energy in MeV above this value. (b) and (c) Probability distribution functions are plotted as contours for $J=60\ \hbar$ ^{158}Er systems with excitation energies of (b) 50 and (c) 300 MeV. The contour intervals are 10% of the maximum value which occur at sphericity for both excitation energies. The distributions were obtained assuming rigid-body moments of inertia.

deformations, it is useful to remember that the coordinates $\gamma=0$, $\beta=0.79$ and $\gamma=\pi/3$, $\beta=0.64$ represent ''superdeformed'' prolate and oblate shapes, respectively, i.e., the ratio of the major to the minor axes is 2. The inertia parameter D is approximately linear in β for small values of β. For larger deformation a linear approximation becomes invalid. The potential energy has a minimum for a spherical system ($\beta=0$) and is approximately independent of γ for small values of β. For larger deformations, the potential energy favors shapes closer to the prolate limit.

In the rotating liquid-drop model and the finite-range liquid-drop model (FRLDM) [22], where the effects of surface diffuseness and the finite range of the nucleus force are added, equilibrium configurations are found which minimize the deformation-plus-rotational energy. Although these models consider a larger number of shape degrees of freedom than the present work, the equilibrium configurations are approximately ellipsoids. These configurations are in fact axially symmetric oblate shapes for all but the largest angular momenta. The corresponding shapes in this work can be obtained by minimizing $V+E^1_{\rm rot}$. A contour plot of this energy is shown in Fig. 2(a) for $J=60\ \hbar$. The minimum energy occurs for an oblate shape ($\gamma=\pi/3$) indicated by the filled dot in the figure. Both the shape and the value of $V+E^1_{\rm rot}$ are similar to the predictions of the RLDM in this example. The equilibrium shape distribution functions for this system with excitation energies of 100 and 300 MeV are shown by the contours in Figs. 2(b) and 2(c), respectively. The distributions have maxima at $\beta=0$ consistent with Eq. (30). The level-density parameter used here and in all other calculations is $a=A/10\ {\rm MeV}^{-1}$. Both distributions have similar features with the exception that, for the higher excitation energy, the distribution extends out to larger values of β. Note that the minimum $V+E^1_{\rm rot}$ energy configuration is not any more characteristic of the compound nucleus shape than is a spherical system or a prolate deformation. Although this oblate configuration has one principal axis about which the rotational energy is lower than the spherical value, the rotational energies about the other axes are larger, contributing less to the distribution function, whereas for nearly spherical systems, all levels contribute approximately equally. Of course for very low excitation energies, the yield will be more localized near the configuration with the minimum rotational-plus-deformation energy, but in this regime shell, pairing, and quantum effects need to be considered.

The dependence of the distributions on angular momentum is illustrated in Fig. 3. This angular-momentum dependence is not strong except at the largest values of J where there is an increased probability of highly deformed prolate-

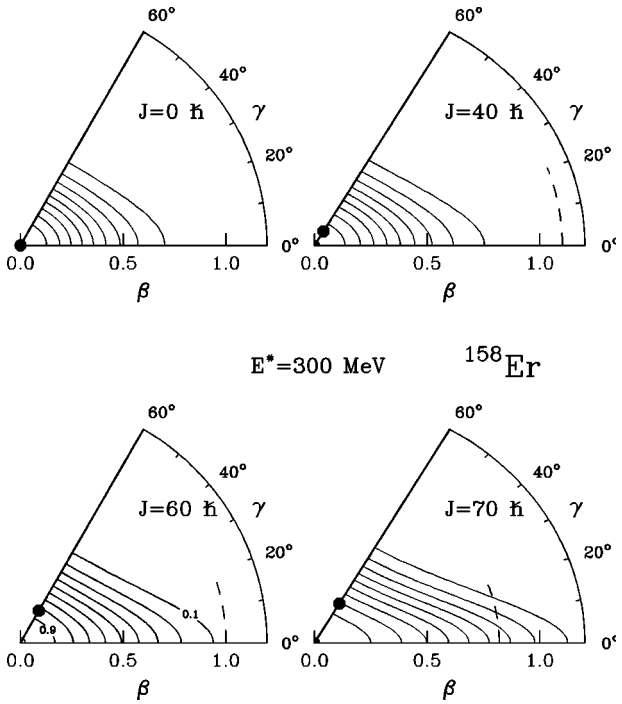

FIG. 3. Predicted probability distribution functions are represented by contour plots for ^{158}Er systems with excitation energy of 300 MeV and with $J=0$, 40, 60, and 70 $\hbar$. The contour interval is 10% of the maximum value which occurs at sphericity. The dashed arcs indicate the approximate location where the fission instability sets in (see text). The filled points indicate the configuration with the minimum rotational-plus-deformation energy as in Fig. 2.

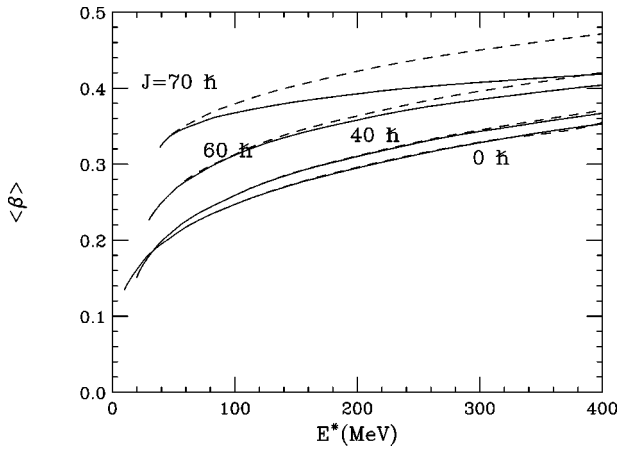

FIG. 4. Predicted dependence of the average value of the β deformation parameter for ^{158}Er systems as a function of the excitation energy. Results are presented for calculations with angular momenta of $J=0$, 40 60, and 70 $\hbar$ and where the shape distributions are unrestricted (dashed curves) or restricted to fission-stable configurations (solid curves). Calculations were performed using rigid-body moments of inertia.

like systems. For $J=70\ \hbar$ the tail of the distribution even extends out to the ($\beta=1.26,\gamma=0$) ''hyperdeformed'' (axis ratio of 3:1) system. It is here where the ellipsoidal-shape parametrization shows its inadequacies, as such prolatelike shapes with the inclusion of a ''neck'' degree of freedom are unstable to the fission, i.e., the fission barrier is only $\sim$5 MeV at this angular momentum. To estimate where fission instabilities are important, a deformation $\beta=\beta_{\rm sad}$ at $\gamma=0$, for which the value of $V+E^1_{\rm rot}$ has the same energy as the angular-momentum dependent saddle-point configuration in the FRLDM, was determined. The values of $\beta_{\rm sad}$ for each angular momentum are indicated by the dashed arcs in Fig. 3. In the following, the compound-nucleus population will be restricted to $\beta<\beta_{\rm sad}$ unless otherwise stated.

The average value of β is plotted as a function of excitation energy in Fig. 4. Results are shown for four values of angular momentum with (solid curve) and without (dashed curve) the condition $\beta<\beta_{\rm sad}$. The average deformation increases both as a function of increasing angular momentum and excitation energy. However, for the case where the compound-nucleus population is restricted to fission-stable shapes ($\beta<\beta_{\rm sad}$), this increase saturates at high values of excitation energy and angular momentum. For $J<60\ \hbar$, the restriction $\beta<\beta_{\rm sad}$ is of little consequence in terms of calculating average properties such as Coulomb-barrier distributions for charged-particle evaporation which are discussed later.

The distributions obtained using moments of inertia associated with irrotational flow are presented in Fig. 5. These distributions show a very strong angular-momentum dependence, with the mean deformation increasing rapidly with J. The moments of inertia for irrotational flow vanish for rota-

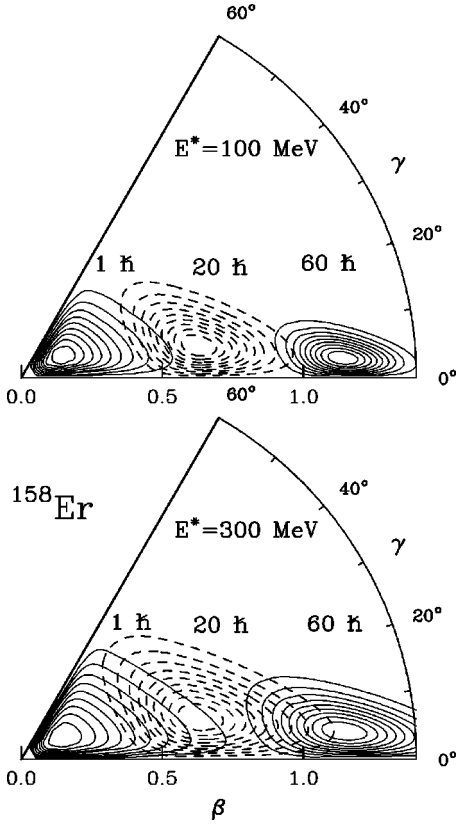

FIG. 5. Predicted probability distribution functions as in Fig. 2, but calculated with moments of inertia associated with irrotational flow. The results were obtained for ^{158}Er systems with the indicated excitation energies and angular momenta.

tions about a symmetry axis, thus preventing such motion as the rotational energy becomes infinite for a fixed angular momentum. As a consequence the population of shapes with axial symmetry ($\beta=0$, $\gamma=0$, and $\gamma=\pi/3$) also vanishes as can be seen in Fig. 5. Although these moments of inertia are not considered appropriate for hot compound nuclei, it does raise a question as to how one should treat spherical and axially symmetric systems, since in a quantum-mechanical treatment, no collective rotations are allowed about a symmetry axis. Of course, the angular momentum can be built up from the intrinsic contributions of each nucleon, however, the level density in this case is expected to be reduced compared to an almost symmetric system with collective rotational levels [11,23–25]. If such reductions in the distribution functions are confined to shapes very close to $\gamma=0$, $\pi/3$, or $\beta=0$ they would have a minimal effect on the average properties of the shape distributions, but this may not be the case. Also it is not clear whether one should think of $\beta=0$ and $\gamma=0$, $\pi/3$ as representing axially symmetric systems. Of the many possible collective degrees of freedom, the formalism of Sec. I projects out the distribution function only on the β and γ coordinates which describe quadrupolelike deformations. Therefore, higher-order deformations should already be summed over and their contributions must be contained in the level density ρ. For example, $\beta=0$ represents distributions of octupole and higher-order deformations. As more of these deformation parameters are explicitly included in the evaluation of the distribution function, the question of how to treat the contribution from spherical and axially symmetric systems may become less important as such systems will represent a decreasing fraction of the total phase space associated with the shape degrees of freedom.

Above a critical angular momentum $L_{\rm I}$ in the RLDM and the FRLDM, the equilibrium configuration with the minimum rotation-plus-deformation energy loses stability against triaxial deformations. For $A>200$, there are no stable triaxial ground-state configurations and the fission barrier also vanishes at $L_{\rm I}$. For lighter systems, a stable triaxial ground-state configuration exists for angular momenta above $L_{\rm I}$ and less than a value $L_{\rm II}$. Also for these lighter systems, the loss of stability against triaxial deformations corresponds closely with the disappearance of the maximum in the distribution function at $\beta=0$. The angular momenta at which the maximum vanishes for nuclei on the line of β stability, calculated from Eq. (30) for temperatures of 2, 3, and 4 MeV, are plotted in Fig. 6 where they are compared to the values of $L_{\rm I}$ and $L_{\rm II}$ determined in the FRLDM. The temperature dependence is not large and the maximum disappears at an angular momentum just before $L_{\rm I}$ for $A<200$. The dependence of the shape distributions in this critical region is illustrated in Fig. 7 for the ^{100}Tc system with angular momenta of 45 and 60 $\hbar$. The configurations with the lowest values of $V+E^1_{\rm rot}$ are again indicated by the solid points. For $J=60\ \hbar$, this configuration is triaxial and this angular momentum is just above $L_{\rm I}$ for this system. At this angular momentum, the fission barrier is 9 MeV and the predicted distribution is still confined to deformations below $\beta_{\rm sad}$. The maximum has moved from $\beta=0$ at 45 $\hbar$ to a prolate deformation on the $\gamma=0$ axis for the higher angular momentum. The distribution now has a local minimum at $\beta=0$. Calculations for higher values of J are problematic as the fission barrier rapidly vanishes and most of the predicted distribution is fission unstable.

It is not the purpose of the present paper to include the ellipsoidal-shape fluctuations into evaporation calculations.

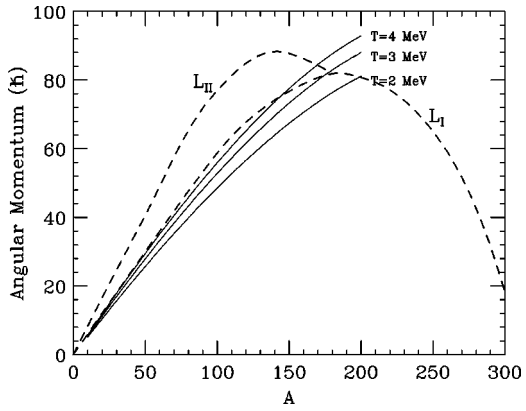

FIG. 6. The variation (solid curves) of the angular momentum at which the maximum in the shape distributions at $\beta=0$ vanishes for β-stable nuclei at the three indicated values of the temperature T. For comparison, the angular momentum $L_{\rm I}$ in the FRLDM at which the ground-state configuration loses stability against triaxial deformation is indicated. For $A>200$, this model predicts the fission barrier is zero, otherwise it is predicted to vanish at the value $L_{\rm II}$.

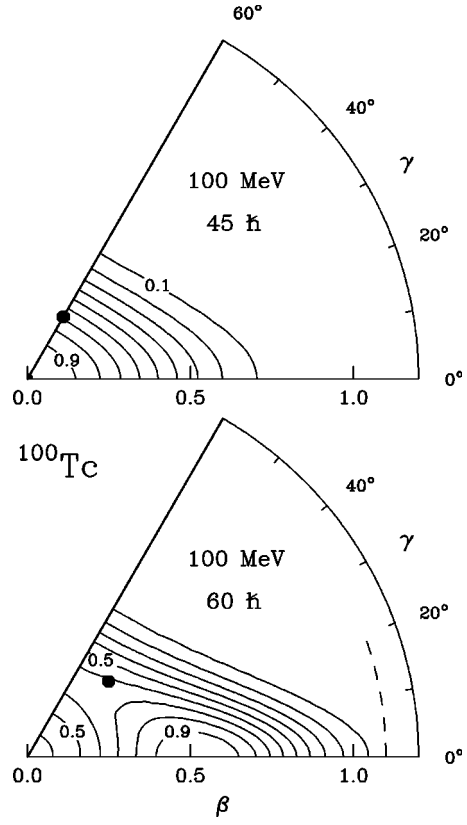

FIG. 7. Contours showing distribution functions as in Fig. 2, but calculated for the ^{100}Tc system at an excitation energy of 100 MeV and angular momenta of 45 and 60 $\hbar$. The configurations with the minimum deformation-plus-rotational energies are again indicated by the solid points.

A new formalism needs to be developed as the treatment of evaporation from spheroidal systems in Ref. [5] is only appropriate for axially symmetric shapes. Care must be taken in the implementation of an extended formalism in a computer code as the spheroidal calculations are already very time consuming. While hopefully these difficulties can be overcome in the future, at present one can look for qualitative differences in the distribution of Coulomb barriers associated with the equilibrium shape distributions. Determining accurately the Coulomb barrier and transmission coefficients for particle evaporation at each point on the surface of a deformed nucleus involves the folding of the nuclear and Coulomb interactions between the evaporated particle and the nucleons of the emitting system with the distributions of these nucleons in the deformed system. This is an involved calculation and often less precise methods are used. In the popular equivalent-spheres approximation [26,27] which was used in the evaporation calculations of Ref. [5], the Coulomb barrier at any point on the surface, with radius R from the center, is obtained from an equivalent spherical system with a radius R. The Coulomb barrier $V_{\rm Coul}$ is thus approximately inversely proportional to R. However, this is rather imprecise as it ignores the multipole moments of the Coulomb field and surface-curvature dependencies of the nuclear potential. For example, the Coulomb barrier for α-particle emission from the tip of a ''superdeformed'' Er prolate system with a ratio of major to minor axes of 2 is $\sim$3 MeV lower than for the result obtained from a more precise folding calculation [28]. The latter folding calculation, which is similar to that outlined in Refs. [29,30], gives the same barrier for emission from a spherical system as the equivalent-sphere approximation.

A much better approximation can be obtained by using the Coulomb potential at a fixed separation s from a sharp-surfaced ellipsoidal system. An analytical expression exists for this potential [31,32] thus permitting rapid calculation of the barrier over the surfaces of all shapes sampled in equilibrium distributions. The separation from the surface was set to $s=3.7$ fm to give a Coulomb barrier of $\sim$18 MeV for emission from a spherical system and the Coulomb barriers obtained for emission from the superdeformed prolate system were within 0.2 MeV of the folding calculation.

Distributions of Coulomb barriers averaged over the surface area of each ellipsoid and then averaged over the thermal distribution of ellipsoids are shown as the solid curves in Fig. 8 for α-particle emission from ^{158}Er systems. In comparison, the dotted curves show distributions obtained for spheroidal-shaped systems using the equilibrium distributions from Ref. [5]. Results are indicated for excitation energies of 100 and 300 MeV and for angular momenta of zero and 60 $\hbar$. With the extra triaxial shape degree of freedom, the Coulomb-barrier distributions for the ellipsoids are wider. The increase in width comes mostly from an increased probability of low Coulomb barriers and thus one would expect this to increase the predicted yield of evaporated low-energy α particles. Similar conclusions can be obtained for other charged particles.

In Ref. [5], the experimental yield of low-energy alpha particles was reproduced for $E^* \lesssim 100$ MeV with only

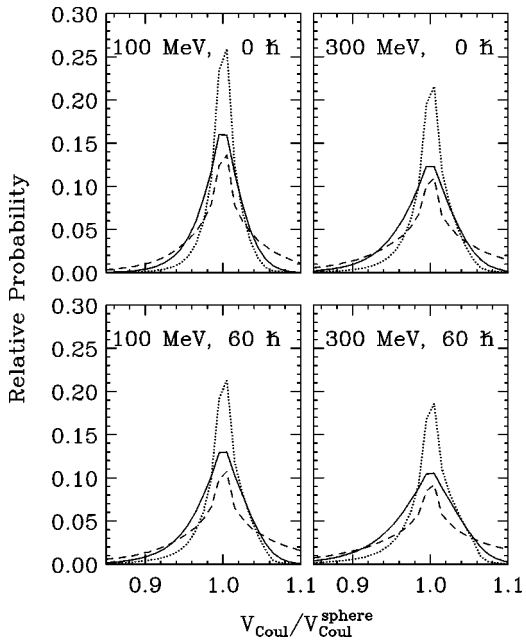

FIG. 8. Distributions of the Coulomb barriers $V_{\rm Coul}$ for α-particle evaporation averaged over the surface area of each shape and over the equilibrium shape distributions. Results are shown for ellipsoidal- (solid curves) and spheroidal- (dotted curves) shape distributions calculated for excitation energies of 100 and 300 MeV and for angular momenta of zero and 60 $\hbar$. $V_{\rm Coul}^{\rm sphere}$ is the Coulomb barrier for the spherical system. The dashed curves are associated with the spheroidal calculations, but where the imprecise equivalent-spheres approximation is used to determined the Coulomb barriers.

spheroidal-shape fluctuations and using the imprecise equivalent-spheres approximation. The Coulomb-barrier distributions obtained with these assumptions are indicated by the dashed curves in Fig. 8. They are closer in shape to the ellipsoidal result (solid source) than the more precise spheroidal result (dotted curves). Therefore, the degree to which the calculations of Ref. [5] reproduced the experiment data is somewhat fortuitous, as the restriction to a single shape degree of freedom was compensated, to an extent, by the use of the equivalent-spheres approximation which overemphasized the effect of deformation. Clearly, shape fluctuations are an important ingredient in understanding the yield of low-energy charged particles. Future evaporation calculations should determine the extent to which they can account for the experimental yield of low-energy charged particles and its excitation-energy dependence. Note, that while the present work has only extended the treatment of shape fluctuations by including one extra shape degree of freedom, explicit consideration of other shapes when determining Coulomb barriers may well further increase the width of the distribution. One then needs to clarify what minimum set of shape variables are required to address this problem.

IV. CONCLUSIONS

A formalism to calculate the equilibrium distribution of ellipsoidally shaped liquid drops has been developed for ap-

plication in the study of hot rotating compound nuclei. The assumptions needed for the derivation of the commonly used metrics associated with the volume element in deformation space are determined. They depend on the deformation dependence of the inertia parameters and the constraints on the angular momenta. Also, these commonly used metrics are only valid for small deformations.

Example probability distribution functions are presented. They are not characterized by any one type of shape in particular, and the full range of deformations from oblate to prolate are populated including spherical and triaxial deformations. However the tail of the distribution extending towards highly deformed prolate configurations is more pronounced especially at the higher angular momenta. For lighter systems there even exists a small window of angular momentum, just before the fission barrier vanishes, for which the shape distributions become more centered around a large prolate deformation.

The Coulomb-barrier distributions for the evaporation of charged particles from the nuclear surface, averaged over the equilibrium distribution of the ellipsoidal shapes, are calculated and compared to similar calculations where the nuclei are restricted to spheroidal shapes only. The distributions associated with the ellipsoidal shapes have enhanced probability for low Coulomb barriers. This could help explain the yield of low-energy α particles observed in the statistical decay of hot compound nuclei.

ACKNOWLEDGMENTS

This work was supported by the Director, Office of High Energy and Nuclear Physics, Nuclear Physics Division of the U.S. Department of Energy under Contract No. DE-FG02-87ER-40316.

[1] Y. Alhassid and B. Bush, Phys. Rev. Lett. **65**, 2527 (1990).
[2] W.E. Ormand, F. Camera, A. Bracco, A. Maj, P.F. Bortignon, B. Million, and R.A. Broglia, Phys. Rev. Lett. **69**, 2905 (1992).
[3] W.E. Ormand, P.F. Bortignon, and R.A. Broglia, Phys. Rev. Lett. **77**, 607 (1996).
[4] D. Kusnezov, Y. Alhassid, and K.A. Snover, Phys. Rev. Lett. **81**, 542 (1998).
[5] R.J. Charity, Phys. Rev. C **61**, 054614 (2000).
[6] S. Levit and Y. Alhassid, Nucl. Phys. **A413**, 439 (1984).
[7] A.L. Goodman, Phys. Rev. C **39**, 2008 (1989).
[8] A.L. Goodman, Nucl. Phys. **A528**, 348 (1991).
[9] F.A. Dodaro and A.L. Goodman, Nucl. Phys. **A596**, 91 (1995).
[10] A. Bohr, K. Dan. Vidensk. Selsk. Mat. Fys. Medd. **26**, 14 (1952).
[11] A. Bohr and B.R. Mottelson, *Nuclear Structure* (Benjamin, New York, 1975), Vol. I.
[12] T. Kaniowska, A. Sobiczewski, K. Pomorski, and S.G. Rohoziński, Nucl. Phys. **A274**, 151 (1976).
[13] K. Kumar and M. Baranger, Nucl. Phys. **A92**, 608 (1967).
[14] S. Cohen and W.J. Swiatecki, Ann. Phys. (N.Y.) **22**, 406 (1963).
[15] B.C. Carlson, J. Math. Phys. **2**, 441 (1966).
[16] B. Remaud and G. Royer, J. Phys. A **14**, 2897 (1981).
[17] G.W. King, R.M. Hainer, and P.C. Cross, J. Chem. Phys. **11**, 27 (1943).
[18] A. Jain and D.G. Thompson, Comput. Phys. Commun. **30**, 301 (1983); **34**, 427 (1985).
[19] S. Cohen, F. Plasil, and W.J. Swiatecki, Ann. Phys. (N.Y.) **82**, 557 (1974).
[20] W.D. Myers and W.J. Swiatecki, Nucl. Phys. **81**, 1 (1966).
[21] W.D. Myers and W.J. Swiatecki, Ark. Fys. **36**, 343 (1967).
[22] A.J. Sierk, Phys. Rev. C **33**, 2039 (1986).
[23] S. Bjørnholm, A. Bohr, and B.R. Mottleson, *Proceedings of the Third International Symposium on the Physics and Chemistry of Fission, Rochester, 1973* (International Atomic Energy Agency, Vienna, 1974), Vol. I, p. 367.
[24] S.E. Vigdor and H.J. Karwowski, Phys. Rev. C **26**, 1068 (1982).
[25] G. Hansen and A.S. Jensen, Nucl. Phys. **A406**, 236 (1983).
[26] R.G. Stokstad and E.E. Gross, Phys. Rev. C **23**, 281 (1981).
[27] J.R. Huizenga, A.N. Behkami, I.M. Govil, W.U. Schröder, and J. Tõke, Phys. Rev. C **40**, 668 (1989).
[28] A.J. Sierk (private comunication).
[29] K.T.R. Davies and J.R. Nix, Phys. Rev. C **14**, 1977 (1976).
[30] P. Möller, J.R. Nix, W.D. Myers, and W.J. Swiatecki, At. Data Nucl. Data Tables **59**, 185 (1995).
[31] J. Binney and S. Tremaine, *Galactic Dynamics* (Princeton University Press, Princeton, NJ, 1987), p. 49.
[32] S. Chandrasekhar, *Ellipsoidal Figures of Equilibrium* (Dover, New York, 1987).